

The red giant branches of Galactic globular clusters in the $(V - I)_0, M_V$ plane: metallicity indices and morphology

Ivo Saviane¹, Alfred Rosenberg^{2,3}, Giampaolo Piotto¹, and Antonio Aparicio⁴

¹ Dipartimento di Astronomia, Università di Padova, vicolo dell’Osservatorio 5, I-35122 Padova, Italy

² Telescopio Nazionale Galileo, vicolo dell’Osservatorio 5, I-35122 Padova, Italy

³ Osservatorio Astronomico di Padova, vicolo dell’Osservatorio 5, I-35122 Padova, Italy

⁴ Instituto de Astrofísica de Canarias, Via Lactea, E-38200 La Laguna, Tenerife, Spain

Received / Accepted

Abstract. The purpose of this study is to carry out a thorough investigation of the changes in morphology of the red giant branch (RGB) of Galactic globular clusters (GGC) as a function of metallicity, in the V, I bands. To this aim, two key points are developed in the course of the analysis.

(a) Using our photometric V, I database for Galactic globular clusters (the largest homogeneous data sample to date; Rosenberg et al. 1999a) we measure a complete set of metallicity indices, based on the morphology and position of the red-giant branch. In particular, we provide here the first calibration of the S , $\Delta V_{1.1}$ and $\Delta V_{1.4}$ indices in the $(V - I, V)$ plane. We show that our indices are internally consistent, and we calibrate each index in terms of metallicity, both on the Zinn & West (1984) and the Carretta & Gratton (1997) scales. Our new calibrations of the $(V - I)_{0,g}$, $\Delta V_{1.2}$, $(V - I)_{-3.0}$ and $(V - I)_{-3.5}$ indices are consistent with existing relations.

(b) Using a grid of selected RGB fiducial points, we define a function in the $(V - I)_0, M_I, [\text{Fe}/\text{H}]$ space which is able to reproduce the whole set of GGC giant branches in terms of a single parameter (the metallicity). As a first test, we show that the function is able to predict the correct trend of our observed indices with metallicity.

The usage of this function will improve the current determinations of metallicity and distances within the Local Group, since it allows to easily map $(V - I)_0, M_I$ coordinates into $[\text{Fe}/\text{H}], M_I$ ones. To this aim the “synthetic” RGB distribution is generated both for the currently used Lee et al. (1990) distance scale, and for the most recent results on the RR Lyr distance scale.

Key words: Stars: abundances - Stars: Population II - Galaxies: abundances - Globular clusters: general

Table 1. The input parameters for the observational sample

NGC	$E_{(B-V)}$	$E_{(V-I)}$	ZW	[Fe/H]		
				CG	RHS97	V_{HB}
104	0.05	0.06	-0.71	-0.70	-0.78	14.05 ± 0.05
288	0.03	0.04	-1.40	-1.07	-1.14	15.40 ± 0.05
362	0.05	0.06	-1.33	-1.15	-1.09	15.51 ± 0.05
1261	0.01	0.01	-1.32	—	-1.08	16.68 ± 0.05
1851	0.02	0.03	-1.23	—	-1.03	16.18 ± 0.05
1904	0.01	0.01	-1.67	-1.37	-1.37	16.15 ± 0.05
3201	0.21	0.27	-1.53	-1.23	-1.24	14.75 ± 0.05
4590	0.04	0.05	-2.11	-1.99	-2.00	15.75 ± 0.10
4833	0.33	0.42	-1.92	-1.58	-1.71	15.70 ± 0.10
5272	0.01	0.01	-1.66	—	-1.33	15.58 ± 0.05
5466	0.00	0.00	-2.22	—	-2.13	16.60 ± 0.05
5897	0.08	0.10	-1.93	-1.59	-1.73	16.30 ± 0.10
5904	0.03	0.04	-1.38	-1.11	-1.12	15.00 ± 0.05
6093	0.18	0.23	-1.75	—	-1.47	16.25 ± 0.05
6171	0.33	0.42	-1.09	—	-0.95	15.65 ± 0.05
6205	0.02	0.03	-1.63	-1.39	-1.33	14.95 ± 0.10
6218	0.19	0.24	-1.40	—	-1.14	14.70 ± 0.10
6254	0.28	0.36	-1.55	-1.41	-1.25	15.05 ± 0.10
6341	0.02	0.03	-2.24	—	-2.10	15.20 ± 0.10
6352	0.21	0.27	-0.50	-0.64	-0.70	15.25 ± 0.05
6362	0.09	0.12	-1.18	-0.96	-0.99	15.35 ± 0.05
6397	0.18	0.23	-1.94	-1.82	-1.76	12.95 ± 0.10
6541	0.12	0.15	-1.79	—	-1.53	15.40 ± 0.10
6637	0.17	0.22	-0.72	—	-0.78	15.95 ± 0.05
6656	0.34	0.44	-1.75	—	-1.41	14.25 ± 0.10
6681	0.07	0.09	-1.64	—	-1.35	15.70 ± 0.05
6723	0.05	0.06	-1.12	—	-0.96	15.45 ± 0.05
6752	0.04	0.05	-1.54	-1.42	-1.24	13.80 ± 0.10
6779	0.20	0.26	-1.94	—	-1.61	16.30 ± 0.05
6809	0.07	0.09	-1.80	—	-1.54	14.45 ± 0.10
7078	0.09	0.12	-2.13	-2.12	-2.02	15.90 ± 0.05

1. Introduction

In very recent times, new determinations of Galactic globular cluster (GGC) metallicities have provided us with new homo-

Send offprint requests to: Ivo Saviane

Correspondence to: saviane@pd.astro.it

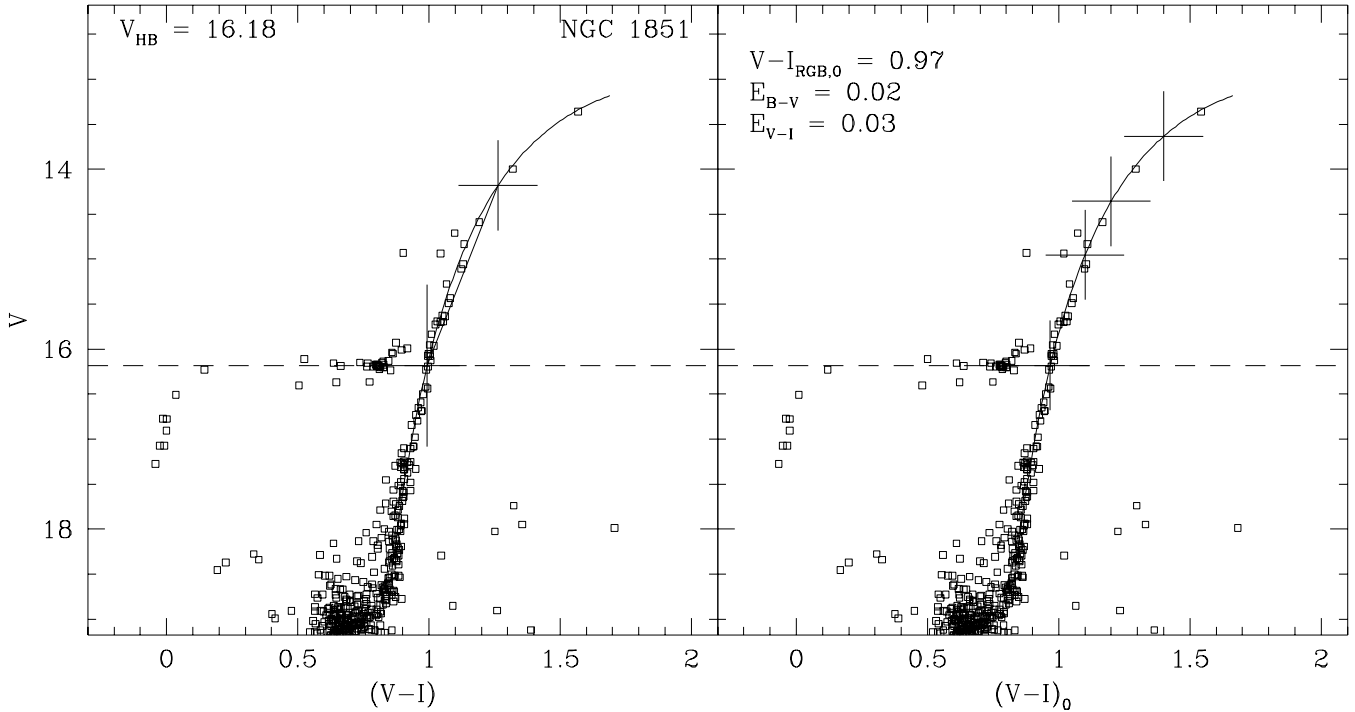


Fig. 1. Graphical representation of the metallicity indices (part 1) that were measured on the selected clusters. (*Left*) The observed CMD of the intermediate-metallicity cluster NGC1851 and its fiducial RGB (solid line). The fiducial locus was obtained by fitting Eq. (1) to the data. The two crosses mark the color of the RGB at the level of the HB, and its color 2 mags brighter than the HB. The slope of the line connecting the two points is the S index. (*Right*) On the color *de-reddened* CMD other four indices are marked. From fainter to brighter magnitudes, the RGB color at the level of the HB, and the V magnitude difference between this point and those at $(V - I)_0 = 1.1, 1.2$ and 1.4 . The dashed line represents the adopted HB level, $V_{\text{HB}} = 16.18$

geneous $[\text{Fe}/\text{H}]$ scales. In particular, Carretta & Gratton (1997; CG) obtained metallicities from high resolution spectroscopy for 24 GGCs, with an internal uncertainty of 0.06 dex. For an even larger sample of 71 GGCs, metallicities have been obtained by Rutledge et al. (1997; RHS97) based on spectroscopy of the CaII infrared triplet. The equivalent widths of the CaII triplet have been calibrated by RHS97 on both the CG scale and the older Zinn & West (1984; ZW) scale. The compilation by RHS97 is by far the most homogeneous one which is currently available.

In the same period, we have been building the largest homogeneous V, I photometric sample of Galactic globular clusters (GGC) based on CCD imaging carried out both with Northern (Isaac Newton Group, ING) and Southern (ESO) telescopes (Rosenberg et al. 1999b, 1999c). The main purpose of the project is to establish the relative age ranking of the clusters, based on the methods outlined in Saviane et al. (1997, 1999b; SRP97, SRP99) and Buonanno et al. (1998; B98). The results of this investigation are presented in Rosenberg et al. (1999a; RSPA99). Here suffice it to say that for a set of 52 clusters we obtained V vs. $(V - I)$ color-magnitude diagrams (CMD), which cover a magnitude range that goes from a few mags below the turnoff (TO) up to the tip of the red giant branch (RGB).

At this point both a spectroscopic and photometric homogeneous databases are available: the purpose of this study is to

exploit them to perform a thorough analysis of the morphology of the RGB as a function of the cluster's metallicity. As a first step, we want to obtain a new improved calibration of a few classical photometric metallicity indices. Secondly, we want to provide to the community a self-consistent, **analytic**, family of giant branches, which can be used in the analysis of old stellar populations in external galaxies.

1.1. Metallicity indices

Photometric indices have been widely used in the past to estimate the mean metallicities of those stellar systems where direct determinations of their metal content are not feasible. In particular, they are used to obtain $[\text{Fe}/\text{H}]$ values for the farthest globulars and for those resolved galaxies of the Local Group where a significant Pop II is present (e.g. the dwarf spheroidal galaxies).

The calibration of V, I indices is particularly important, since with comparable exposure times, deeper and more accurate photometry can be obtained for the cool, low-mass stars in these broad bands than in B, V . Moreover, our huge CMD database allows a test of the new CG scale on a large basis: we are able to compare the relations obtained for both the old ZW and new scale, and check which one allows to rank GGCs in the most accurate way. Indeed, the most recent calibration of

the V, I indices (Carretta & Bragaglia 1998) is based on just 8 clusters.

1.2. Old stellar populations in Local Group galaxies

A reliable metallicity ranking of GGC giant branches also allows studies that go beyond a simple determination of the *mean* metallicity of a stellar population. As an illustration, we may recall the recent investigation of the halo metallicity distribution function (MDF) of NGC 5128 (Harris et al. 1999), which was based on the fiducial GC lines obtained by Da Costa & Armandroff (1990, hereafter DA90). These studies can be made more straightforward by providing a suitable analytic representation of the RGB family of GGCs. Indeed, assuming that most of the GGCs share a common age (e.g. Rosenberg et al. 1999a), one expects that there should exist a “universal” function of $\{(V - I)_0, M_I, [\text{Fe}/\text{H}]\}$ able to map any $[(V - I)_0, M_I]$ coordinate pair into the corresponding metallicity (provided that an independent estimate of the distance and extinction of the star are available). We will show here that such relatively simple mono-parametric function can actually be obtained, and that this progress is made possible thanks to the homogeneity of both our data set and analysis.

In order to enforce a proper use of our calibrations, we must clearly state that, in principle, the present relations are valid only for rigorously old stellar populations (i.e. for stars as old as the bulk of Galactic globulars). At fixed abundance, giant branches are somewhat bluer for younger ages (e.g. Bertelli et al. 1994). Moreover, in real stellar systems AGB stars are also present on the blue side of the RGB (cf. Fig. 2). Both effects must be taken into account when dealing with LG galaxies, since they could lead to systematic effects in both the mean abundances and the abundance distributions (e.g. Saviane et al. 1999a).

1.3. Layout of the paper

The observational sample, on which this investigation is based, is presented in Sect. 2. Sect. 3 is devoted to the set of indices which are to be calibrated. They are defined in Sect 3.1. The reliability of our sample is tested in Sect. 3.3, where we demonstrate that our methodology produces a set of well-correlated indices. In Sect. 4 we show that, once a distance scale is assumed for the GGCs, our whole set of RGBs can be approximated by a *single* analytic function, which depends on the metallicity alone. This finding allows a new and easier way to determine the distances and mean metallicities of the galaxies of the Local Group, extending the methods of Da Costa & Armandroff (1990), and Lee et al. (1993). The metallicity indices are calibrated in Sect. 6, where analytic relations are provided both for the ZW and for the CG scales. Using these indices, we are able to test our analytic RGB family in Sect 7. Our conclusions are in Sect. 8.

2. The observational sample

Thirty-nine clusters have been observed with the ESO/Dutch 0.9m telescope at La Silla, and 16 at the RGO/JKT 1m telescope in la Palma. This database comprises 75% of the GGC whose distance modulus is $(m - M)_V < 16$. The zero-point uncertainties of our calibrations are < 0.03 mag for each band. Three clusters were observed both with the southern and the northern telescopes, thus providing a consistency check of the calibrations: no systematic differences were found, at the level of accuracy of the zero-points. A detailed description of the observations and reduction procedures will be given in forthcoming papers (Rosenberg et al. 1999b, 1999c) presenting the single clusters.

A subsample of this database was used for the present investigation. We retained those clusters whose CMD satisfied a few criteria: (a) the HB level could be well determined; (b) the RGB was not heavily contaminated by foreground/background contamination; and (c) the RGB was well defined up to the tip. This subsample largely overlaps that used for the age investigation, but a few clusters whose TO position could not be measured, are nevertheless useful for the metallicity indices definition. Conversely, in a few cases the lower RGB could be used for the color measurements, while the upper branch was too scarcely defined for a reliable definition of the fiducial line. Two of the CMDs that were used are shown in Figs. 1 (NGC 1851) and 2 (NGC 104), and they illustrate the good quality of the data.

The dataset of 31 clusters used in this paper is listed in Table 1. From left to right, the columns contain the NGC number, the reddening both in $(B - V)$ and $(V - I)$, the metallicity according to three different scales, and the apparent magnitude of the horizontal branch (HB). The $E_{(B-V)}$ values were taken from the Harris (1996) on-line table¹. The $(V - I)$ reddenings were obtained by assuming that $E_{(V-I)} = 1.28 \times E_{(B-V)}$ (Dean et al. 1978). The values of the metallicity were taken from RHS97: they represent the equivalent widths of the CaII infrared triplet, calibrated either onto the Zinn & West (1984) scale (ZW column) or the Carretta & Gratton (1997) scale (RHS97 column). Moreover, the original Carretta & Gratton metallicities (CG column) are also given for the clusters comprised in their sample.

The HB level was found in different ways for clusters of different metallicity. For the the metal rich and metal intermediate clusters, a magnitude distribution of the HB stars was obtained, and the mode of the distribution was taken. Where the HB was too scarcely populated, a horizontal line was fitted through the data. The blue tail of the metal poorest clusters does not reach the horizontal part of the branch: in that case, a fiducial HB was fitted to the tail, and the magnitude of the horizontal part was taken as the reference level. The fiducial branch was defined by taking a cluster having a bimodal HB color distribution (NGC 1851, cf. Fig. 1) and then extending its HB both to the red and to the blue by “appending” clusters being more and more metal rich and metal poor, respectively.

¹ <http://physun.physics.mcmaster.ca/Globular.html>

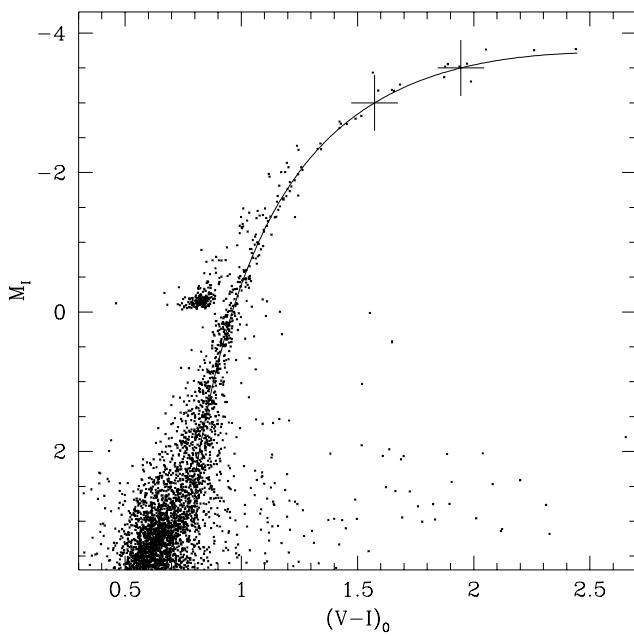


Fig. 2. Graphical representation of the metallicity indices (part 2) that were measured on the selected clusters. In this figure, the absolute CMD of the metal rich cluster NGC 104 is plotted in the $(V - I)_0, M_I$ plane, adopting an apparent distance modulus $(m - M)_V = 13.35$ and a reddening $E_{V - I} = 0.06$ (see text for the discussion). This plot shows the ability of the analytic function to reproduce even the more extended RGBs. The two crosses mark the color of the RGB at $M_I = -3.0$ and $M_I = -3.5$.

The details of this procedure, as well as the errors associated to the V_{HB} in Table 1, are discussed in RSPA99. For NGC 1851, $V_{\text{HB}} = 16.18 \pm 0.05$ was adopted (dashed line in Fig. 1), and this value is just 0.02 mag brighter than the value found by Walker (1992) and Saviane et al. (1998).

Based on this observational sample, a set of metallicity indices were measured on the RGBs of the clusters. In the next section, the indices are defined and the measurement procedures are described. Consistency checks are also performed.

3. Metallicity indices

3.1. Definitions

The metallicity indices calibrated in this study are represented and defined in Fig. 1 and Fig. 2. The figures represent the CMD of NGC 1851 and NGC 104 in different color-magnitude planes, and the crosses mark the position of the RGB points used in the measurement of the indices.

The left panel of Fig. 1 shows the apparent colors and magnitudes for NGC 1851: the inclined line helps to identify the first index, S . This was defined, in the $(B - V, V)$ plane, by Hartwick (1968) as the slope of the line connecting two points on the RGB: the first one at the level of the HB, and the second one 2.5 mag brighter. We use the same definition for the

$(V - I, V)$ plane here; however, in order to be able to use our metal richest clusters, we redefined S by measuring the second RGB point 2 mag brighter than the HB. Since S is measured on the apparent CMD, it is independent both from the reddening and the distance modulus.

The right panel of the same figure, shows the apparent V magnitude vs. the de-reddened $(V - I)_0$ color. In this panel, four other indices are identified, i.e. $(V - I)_{0,g}$, $\Delta V_{1.1}$, $\Delta V_{1.2}$, and $\Delta V_{1.4}$. The first one is the RGB color at the level of the HB, and the other three measure the magnitude difference between the HB and the RGB at a fixed color $(V - I)_0 = 1.1, 1.2$ and 1.4 mag. The former index was originally defined by Sandage & Smith (1966) and the latter one by Sandage & Wallerstein (1960), in the $(B - V)_0, V$ plane. The other two indices, $\Delta V_{1.1}$ and $\Delta V_{1.2}$, are introduced later to measure the metal richest GCs. These indices require an independent color excess determination.

Finally, Fig. 2 shows the CMD of NGC 104 (47 Tuc) in the absolute $(V - I)_0, M_I$ plane: the adopted distance modulus, $(m - M)_V = 13.35$, was obtained by correcting the apparent luminosity of the HB according to Lee et al. (1990; cf. Sect. 6). By comparison, Harris' catalog reports $(m - M)_V = 13.32$. Two other indices are represented in the figure: $(V - I)_{-3.0}$ and $(V - I)_{-3.5}$. They are defined as the RGB color at a fixed absolute I magnitude of $M_I = -3.0$ (Da Costa & Armandroff 1990) or $M_I = -3.5$ (Lee et al. 1993). The latter index was also discussed by Armandroff et al. (1993), and a calibration formula was given in Caldwell et al. (1998). This is based on the DA90 clusters plus M5 and NGC 362 from Lloyd Evans (1983).

Since these two indices are defined on the bright part of the RGB, they can be measured even for the farthest objects of the Local Group (LG). Due to the fast luminosity evolution of the stars on the upper RGB, this part of the branch was typically under-sampled by the early small-size CCDs, so no wide application of these indices has been made for Galactic globulars. However, this is of no concern for galaxy-size stellar systems. It will be shown in Sect. 6 that good accuracies can be obtained even for GCs, provided that the analytic function of Eq. (1) is used.

3.2. Measurement procedures

Colors and magnitudes were measured on a fiducial RGB, which has been found by least-square fitting an analytic function to the observed branch. After some experimenting, it was found that the best solution is to use the following relation:

$$y = a + bx + c/(x - d) \quad (1)$$

where x and y represent the color and the magnitude, respectively. One can see from Figs. 1 and 2 that the function is indeed able to represent the giant branch over the typical metallicity range of globular clusters. Moreover, it is shown in Sect. 4 that, when the CMDs are corrected for distance and reddening, the four coefficients can be parametrized as a function of $[\text{Fe}/\text{H}]$, so that one is able to reproduce the RGB of each cluster, using

Table 2. The measured metallicity indices

NGC	$(V - I)_{0,g}$	S	ΔV		$(V - I)$		$\log_{10}((V - I)_{0,g})$
			1.1	1.2	1.4	@3.5	
104	0.99	4.13	0.78	1.27	1.87	1.94	1.57
288	0.95	6.39	1.25	1.75	2.36	1.51	1.35
362	0.90	7.28	1.67	2.09	2.57	1.45	1.28
1261	0.91	7.77	1.62	2.13	2.73	1.39	1.25
1851	0.97	7.41	1.23	1.82	2.55	1.45	1.31
1904	0.94	8.56	1.58	2.14	2.83	1.35	1.24
3201	0.99	8.72	1.19	1.91	2.71	1.39	1.27
4590	0.91	9.98	1.90	2.52	3.25	1.24	1.16
4833	0.92	9.25	1.80	2.36	3.12	1.28	1.19
5272	0.91	7.60	1.66	2.13	2.81	1.36	1.24
5466	0.91	9.85	1.93	2.50	3.18	1.24	1.16
5897	0.97	8.73	1.34	2.00	2.79	1.35	1.25
5904	0.93	6.91	1.41	1.91	2.55	1.44	1.30
6093	0.93	8.02	1.58	2.12	2.91	1.34	1.24
6171	1.07	5.66	0.31	1.09	1.93	1.67	1.49
6205	0.89	7.70	1.75	2.20	2.75	1.37	1.23
6218	0.95	7.09	1.34	1.88	2.51	1.46	1.31
6254	0.90	8.25	1.75	2.29	3.17	1.30	1.21
6341	0.88	9.92	2.15	2.69	3.40	1.21	1.13
6352	1.12	3.11	-0.16	0.52	1.30	1.99	1.75
6362	0.93	5.84	1.31	1.76	2.32	1.55	1.37
6397	0.89	9.45	1.98	2.49	3.12	1.26	1.16
6541	1.01	8.59	1.03	1.77	2.67	1.39	1.29
6637	0.96	4.39	0.96	1.41	1.97	1.82	1.53
6656	0.86	10.32	2.27	2.69	2.96	1.24	1.12
6681	0.95	7.54	1.35	1.92	2.76	1.37	1.27
6723	1.01	6.02	0.76	1.38	2.18	1.55	1.41
6752	0.99	7.16	1.08	1.69	2.46	1.45	1.33
6779	0.94	8.74	1.60	2.18	2.94	1.32	1.22
6809	0.93	9.38	1.72	2.29	2.87	1.32	1.20
7078	0.88	9.82	2.10	2.62	3.27	1.23	1.14

just one parameter: the metallicity. At any rate, the indices were measured on the original loci, so that an independent check of the goodness of the generalized hyperbolae can be made, by comparison of the measured vs. predicted indices.

All the indices' values that have been measured are reported in Table 2. In this table, the cluster NGC number is given in column 1; the following columns list, from left to right, $(V - I)_{0,g}$, S , $\Delta V_{1,1}$, $\Delta V_{1,2}$, $\Delta V_{1,4}$, and finally the RGB color measured at $M_I = -3$ and -3.5 . The Lee et al. (1990) distance scale was used to compute the last two indices (cf. Sect. 6).

3.3. Internal consistency checks

Before discussing the indices as metallicity indicators, we checked their internal consistency. We will show in Sect. 6 that the index S is the most accurate one, as expected, since it does not require reddening and distance corrections. The rest of the indices are therefore plotted vs. S in Figs. 3 and 4, and we expect that most of the scatter will be in the vertical direction.

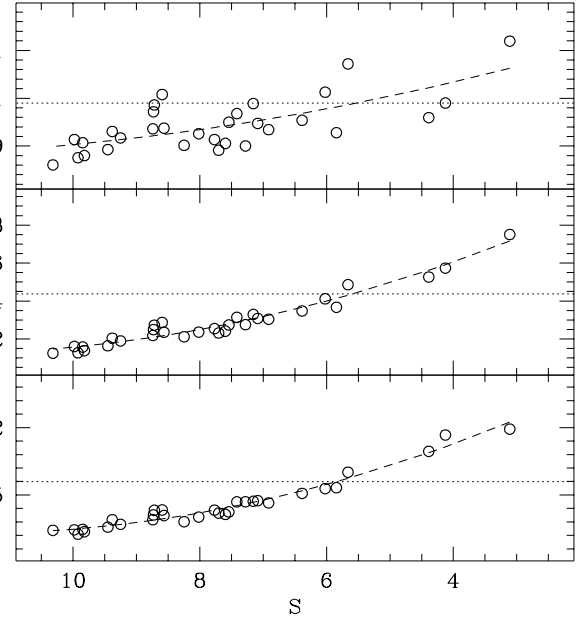


Fig. 3. The metallicity indices $(V - I)_{0,g}$, $(V - I)_{-3.0}$, and $(V - I)_{-3.5}$ are plotted as a function of the index S . The points are ordered such that the metal-poor to metal-rich cluster sequence goes from left to right. The very good correlations between $(V - I)_{-3.0}$, $(V - I)_{-3.5}$ and S (the rms of the parabolic fits are 2% and 3% respectively), demonstrate that these indices are very accurate

Second order polynomials were fitted to the distributions, and the rms of the fit was computed for each index. In order to intercompare the different indices, a relative uncertainty has been computed by dividing the rms by the central value of each parameter (this value is identified by a dotted line in each figure).

In this way, the scatter of the metal index i is $\Delta i/i = 0.02$, 0.02, 0.04, 0.06, 0.12, and 0.26, for the indices $(V - I)_{-3}$, $(V - I)_{-3.5}$, $(V - I)_{0,g}$, $\Delta V_{1,4}$, $\Delta V_{1,2}$, and $\Delta V_{1,1}$, respectively. These values confirm the visual impression of the figures, that $\Delta(V - I)_{-3.0}$ and $\Delta(V - I)_{-3.5}$ are the lowest dispersion indices, followed by $(V - I)_{0,g}$ and $\Delta V_{1,4}$.

The indices will be calibrated in terms of [Fe/H] in Sect. 6; however, before moving to this section, we want to present a new way to provide "standard" GGC branches in the $(V - I)_0, M_I$ plane, along the lines of the classical Da Costa & Armandroff (1990) study. Using this family of RGB branches, we are able to make predictions on the trend of the already defined indices with metallicity; these trends can thus be compared to the observed ones, and therefore provide a further test of the reliability of our RGB family (cf. Sect 7).

4. New standard globular cluster giant branches

Da Costa & Armandroff (1990) presented in tabular form the fiducial GGC branches of 6 globulars, covering the metallicity range $-2.17 \leq [\text{Fe}/\text{H}] \leq -0.71$. The RGBs were cor-

Table 3. Clusters selected for the determination of the analytic fits, listed for increasing [Fe/H] values

Cluster	V_{HB}	$E_{(B-V)}$	$E_{(V-I)}$	[Fe/H] _{ZW}	[Fe/H] _{RCCG}	[Fe/H] _{CG}
NGC 104	14.05	0.050	0.064	-0.71	-0.78	-0.70
NGC 5904	15.00	0.023	0.029	-1.38	-1.12	-1.11
NGC 288	15.40	0.036	0.046	-1.40	-1.14	-1.07
NGC 6205	14.95	0.000	0.000	-1.63	-1.33	-1.39
NGC 5272	15.58	0.002	0.003	-1.66	-1.33	—
NGC 6341	15.20	0.010	0.013	-2.24	-2.10	—

Table 4. The fiducial points for the 6 selected clusters

NGC 104		NGC 288		NGC 5272		NGC 5904		NGC 6205		NGC 6341	
I	$(V-I)$	I	$(V-I)$	I	$(V-I)$	I	$(V-I)$	I	$(V-I)$	I	$(V-I)$
13.782	0.978	15.359	0.914	15.492	0.852	14.725	0.926	14.645	0.867	15.060	0.852
13.604	0.994	15.107	0.939	15.151	0.874	14.457	0.942	14.322	0.890	14.720	0.872
13.443	1.008	14.849	0.960	14.789	0.892	14.221	0.961	14.033	0.909	14.395	0.894
13.317	1.021	14.593	0.984	14.597	0.910	14.040	0.978	13.788	0.929	14.079	0.916
13.075	1.045	14.342	0.999	14.359	0.929	13.878	0.994	13.595	0.944	13.789	0.937
12.862	1.070	14.109	1.018	14.143	0.955	13.700	1.009	13.381	0.966	13.533	0.953
12.619	1.101	13.881	1.036	13.796	0.990	13.456	1.032	13.170	0.984	13.303	0.974
12.346	1.136	13.649	1.062	13.517	1.021	13.190	1.061	12.984	1.005	13.082	0.994
12.035	1.185	13.376	1.090	13.265	1.046	12.916	1.091	12.832	1.019	12.850	1.020
11.761	1.231	13.058	1.132	13.005	1.076	12.655	1.122	12.631	1.045	12.611	1.039
11.461	1.281	12.766	1.173	12.759	1.110	12.419	1.154	12.363	1.077	12.351	1.067
11.101	1.362	12.534	1.210	12.519	1.148	12.231	1.183	12.118	1.111	12.075	1.102
10.696	1.459	12.380	1.233	12.302	1.187	12.073	1.212	11.945	1.138	11.771	1.148
10.330	1.600	12.163	1.268	12.109	1.227	11.868	1.254	11.844	1.156	11.492	1.195
10.062	1.720	11.928	1.317	11.878	1.275	11.615	1.305	11.707	1.178	11.284	1.233
9.877	1.856	11.617	1.411	11.741	1.310	11.335	1.371	11.571	1.204	11.154	1.265
9.706	2.019	11.427	1.483	11.575	1.344	11.116	1.422	11.395	1.252	11.008	1.295
9.602	2.148	—	—	11.494	1.377	10.902	1.489	11.141	1.312	10.854	1.320
9.524	2.315	—	—	11.330	1.406	10.652	1.585	10.870	1.376	10.709	1.351
9.573	2.576	—	—	11.240	1.447	10.457	1.680	10.643	1.444	—	—
9.619	2.768	—	—	11.112	1.488	10.343	1.742	10.552	1.492	—	—
—	—	—	—	11.078	1.528	—	—	—	—	—	—
—	—	—	—	11.047	1.546	—	—	—	—	—	—

rected to the absolute $(V-I)_0, M_I$ plane using the apparent V magnitude of the HB, and adopting the Lee et al. (1990) theoretical HB luminosity. Since the DA90 study, these branches have been widely used for stellar population studies in the Local Group. Based on these RGBs, in particular, a method to determine both the distance and mean metallicity of an old stellar population was presented by Lee et al. (1993).

Both DA90 and Lee et al. (1993) provided a relation between the metallicity [Fe/H] and the color of the RGB at a fixed absolute I magnitude ($M_I = -3$ and -3.5 , respectively), and recently a new relation for $(V-I)_{-3.5}$ has also been obtained by Caldwell et al. (1998). Once the distance of the population is known (e.g. via the luminosity of the RGB tip), then an estimate of its *mean* metallicity can be obtained using one of the calibrations. It is assumed that the age of the population is comparable to that of the GGCs, and that the age spread is negligible compared to the metallicity spread (RSPA99).

In such case, one expects that any RGB star's position in the absolute CMD is determined just by its metallicity, and that a better statistical determination of the population's metal content would be obtained by converting the color of *each* star into a [Fe/H] value. With this idea in mind, in the following sections we will show that this is indeed possible, at least for the bright/most sensitive part of the giant branch. We found that a relatively simple *continuous* function can be defined in the $(V-I)_0, M_I, [\text{Fe}/\text{H}]$ space, and that this function can be used to transform the RGB from the $(V-I)_0, M_I$ plane to the $[\text{Fe}/\text{H}], M_I$ plane.

In order to obtain this function, we first selected a subsample of clusters with suitable characteristics, so that a reference RGB grid can be constructed. The fiducial branches for each cluster were then determined in an objective way, and they were corrected to the absolute $((V-I)_0, M_I)$ plane. In this plane,

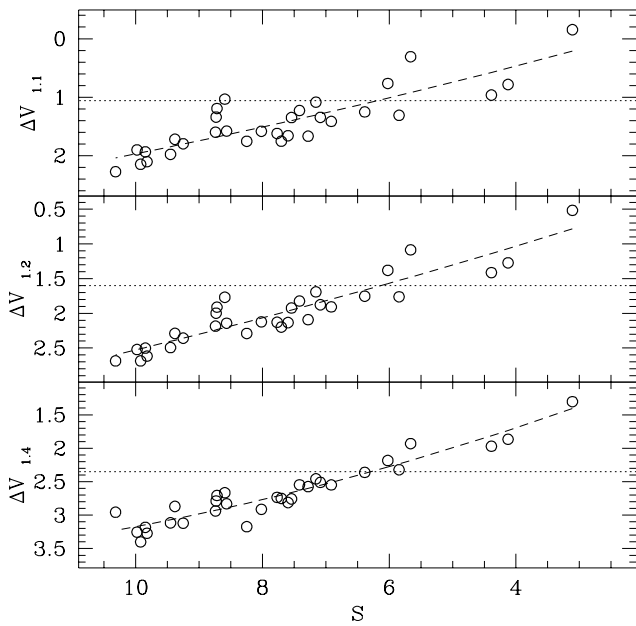


Fig. 4. The metallicity indices $\Delta V_{1.1}$, $\Delta V_{1.2}$, and $\Delta V_{1.4}$ as a function of the index S . The points are ordered such that the metal-poor to metal-rich cluster sequence goes from left to right. The dashed line represents a second order polynomial least-square fitted to the data. The typical relative uncertainty on each index has been estimated by taking the ratio of the *rms* of the fit over the value of the parameter at the level of the horizontal dotted line

the analytic function was fitted to the RGB grid. These operations are described in the following sections.

4.1. Selection of clusters

The clusters that were used for the definition of the fiducial RGBs are listed in Table 3, in order of increasing metallicity. The table reports the cluster name, and some of the parameters listed in Table 1 are repeated here for ease of use. The values of the reddening were in some cases changed by a few thousandth magnitudes (i.e. well within the typical uncertainties on $E_{(B-V)}$), to obtain a sequence of fiducial lines that move from bluer to redder colors as $[\text{Fe}/\text{H}]$ increases, and again the corresponding $E_{(V-I)}$ values were obtained assuming that $E_{(V-I)} = 1.28 \times E_{(B-V)}$ (Dean et al. 1978). Indeed, due to the homogeneity of our sample, we expect that if a monotonic color/metallicity sequence is not obtained, then only the uncertainties on the extinction values must be taken into account.

In order to single out these clusters from the total sample, some key characteristics were taken into account. In particular, we considered clusters whose RGBs are all well-defined by a statistically significant number of stars; they have low reddening values ($E_{(B-V)} \leq 0.05$); and they cover a metallicity range that includes most of our GGCs ($-2.2 \leq [\text{Fe}/\text{H}] \leq -0.7$ on the ZW scale).

The DA90 fiducial clusters were NGC 104, NGC 1851, NGC 6752, NGC 6397, NGC 7078 and NGC 7089 (M2). NGC 104 is the only cluster in common with the previous study, and M2 is not present in our dataset. The other objects have been excluded from our fiducial sample since they have too large reddening values ($E_{(B-V)} > 0.05$ for NGC 6397 and NGC 7078), or their RGBs are too scarcely populated in our CMDs (NGC 1851 and NGC 6752). Nevertheless, the calibrations that we obtain for the $(V-I)_{-3.0}$ and $(V-I)_{-3.5}$ are in fairly good agreement with those obtained by DA90 (for the small discrepancies at the high metallicity end, cf. Sect. 6.2 and 6.3), and in particular with the recent Caldwell et al. (1998) calibration for the $(V-I)_{-3.5}$ index.

4.2. Determination of the fiducial loci

The ridge lines of our fiducial RGBs were defined according to the following procedure. The RGB region was selected from the calibrated photometry, by excluding both HB and AGB stars. All stars bluer than the color of the RR Lyr gap were removed; AGB stars were also removed by tracing a reference straight line in the CMD, and by excluding all stars blue-side of this line. This operation was carried out in the $((V-I), I)$ plane, where the RGB curvature is less pronounced, and a straight line turns out to be adequate.

The fiducial loci were then extracted from the selected RGB samples. The $(V-I)$ and I vectors were sorted in magnitude, and bins were created containing a given number of stars. Within each bin, the median color of the stars and the mean magnitude were used as estimators of the bin central color and brightness. The number of stars within the bins was exponentially increased going from brighter to fainter magnitudes. In this way, (a) one can use a small number of stars for the upper RGB, so that the color of the bin is not affected by the RGB slope, and (b) it is possible to take advantage of the better statistics of the RGB base. Finally, the brightest two stars of the RGB were not binned, and were left as representatives of the top branch. After some experimenting, we found that a good RGB sampling can be obtained by taking for each bin a number of stars which is proportional to $e^{0.2 \cdot i}$, where i is an integer number. The resulting fiducial vectors were smoothed using an average filter with a box size of 3.

The RGB regions of the 6 clusters are shown in Fig. 5, together with the fiducial lines: it can be seen that in all cases the AGBs are easily disentangled from the RGBs. The values of the fiducial points corresponding to the solid lines in Fig. 5, are listed in Table 4.

4.3. Analytic fits to the fiducial loci

The fiducial branches defined in Sect. 4.2 were fitted with a parametrized family of hyperbolae. First, the RGBs were moved into the absolute $(V-I)_0, M_I$ plane. The distance modulus was computed from the apparent magnitude of the HB (cf. Table 3) and by assuming the common law $M_V(\text{HB}) = a[\text{Fe}/\text{H}] + b$; in order to compare our results with those of

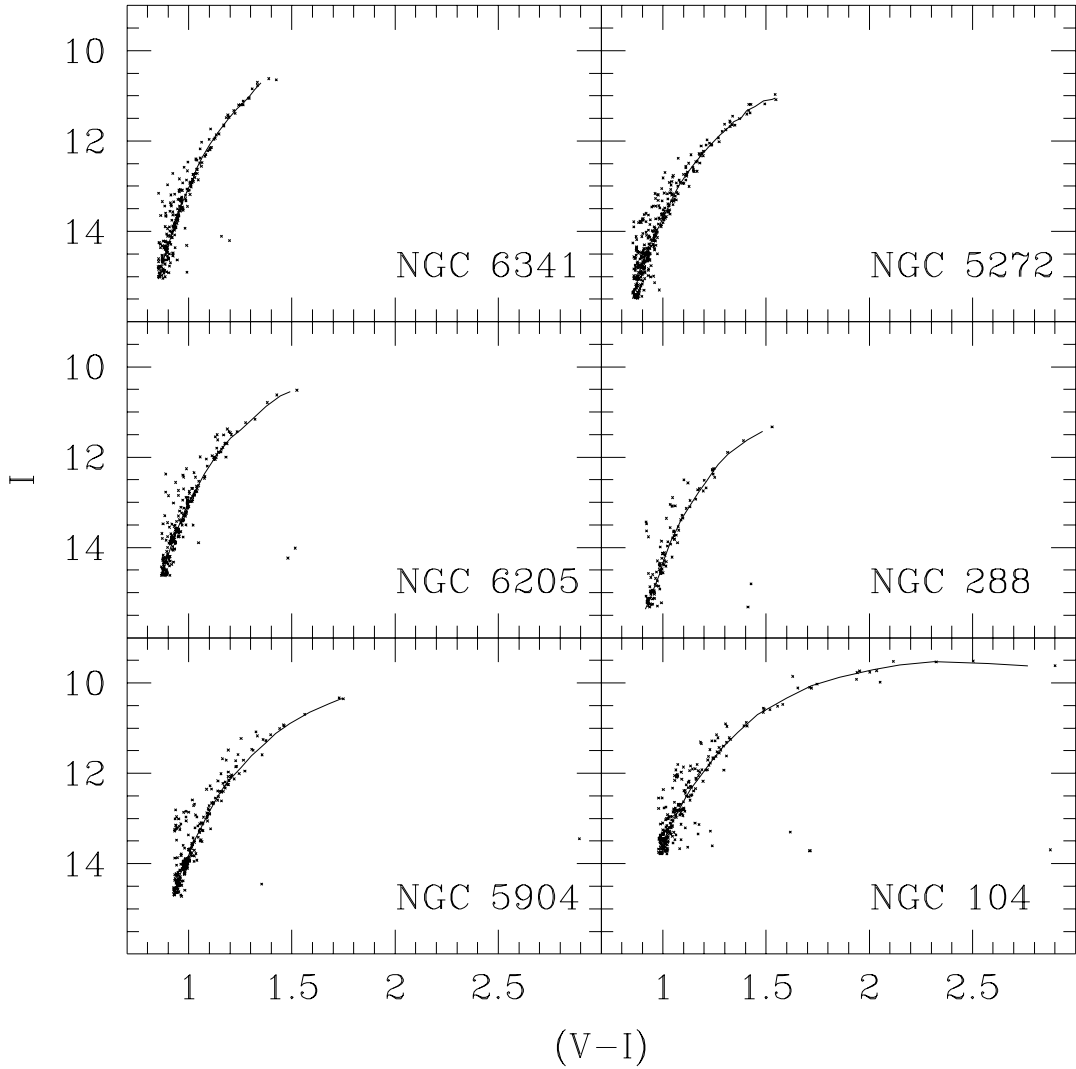


Fig. 5. The RGBs of the selected clusters (crosses) and their fiducial lines (solid curves). The clusters are represented, from left to right and top to bottom, in order of increasing metallicity

DA90, $a = 0.17$ and $b = 0.82$ were used, but we also obtained the same fits using more recent values as in Carretta et al. (1999), i.e. $a = 0.18$ and $b = 0.90$. The RGB was modeled with an hyperbola as in Rosenberg et al. (1999a), but in this case the coefficients were taken as second order polynomials in $[\text{Fe}/\text{H}]$. In other words, we parametrized the whole family of RGBs in the following way:

$$M_I = a + b \cdot (V - I) + c / [(V - I) - d] \quad (2)$$

where

$$a = k_1[\text{Fe}/\text{H}]^2 + k_2[\text{Fe}/\text{H}] + k_3 \quad (3)$$

$$b = k_4[\text{Fe}/\text{H}]^2 + k_5[\text{Fe}/\text{H}] + k_6 \quad (4)$$

$$c = k_7[\text{Fe}/\text{H}]^2 + k_8[\text{Fe}/\text{H}] + k_9 \quad (5)$$

$$d = k_{10} \quad (6)$$

The list of the parameters of the fits in magnitude is reported in Table 5, together with the *rms* of the residuals around the fitting curves. The table shows that the parameter d does not depend on the choice of the distance scale, as expected. Even the other coefficients are little dependent on the distance scale, apart from k_3 . It is affected by the zero-point of the HB luminosity-metallicity relation, and indeed there is the expected ~ 0.1 mag difference going from the LDZ to the C99 distance scale.

One could question the choice of a constant d , but after some training on the theoretical isochrones, we found that even allowing for a varying parameter, its value indeed scattered very little around some mean value. This empirical result is a good one, in the sense that it allows to apply a robust linear least-square fitting method for any choice of d , and then to search for the best value of this constant by a simple *rms* minimization. We chose to fit the $M_I = f\{(V - I)_0, [\text{Fe}/\text{H}]\}$ func-

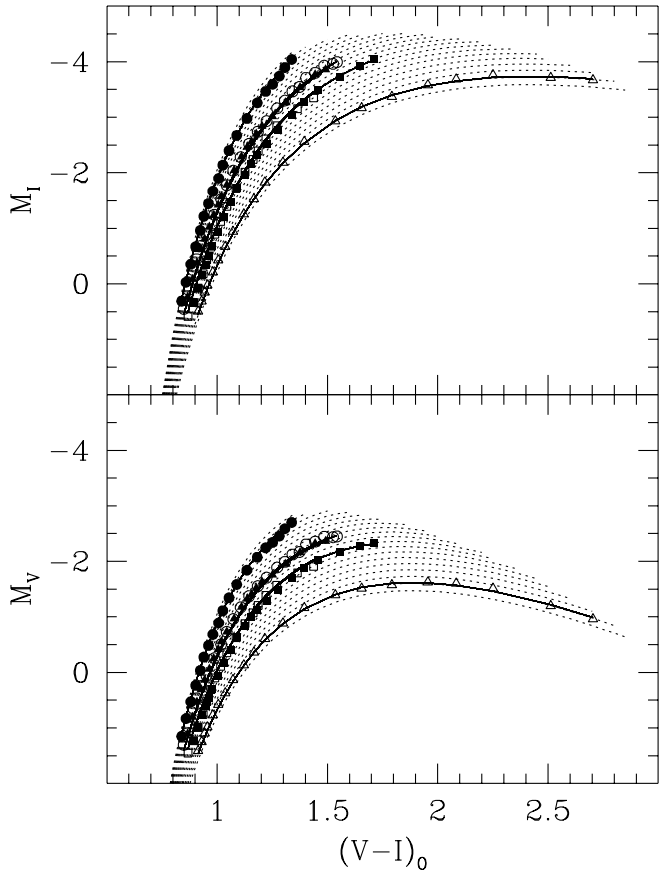


Fig. 6. The fiducial points of our reference sample of 6 clusters plotted over the analytic fits for the ZW metallicity scale. The analytic RGBs (dashed lines) have been calculated at constant $\Delta[\text{Fe}/\text{H}] = 0.2$ dex steps. The observed ridge lines have been corrected for reddening and absorption + distance scale. In the upper panel, the fits in the $V - I, M_I$ plane are shown, while fits in the $V - I, M_V$ plane are shown in the lower panel. Different symbols identify different clusters: NGC 104 (open triangles), NGC 288 (open squares), NGC 5272 (open circles), NGC 5904 (solid squares), NGC 6205 (solid triangles) and NGC 6341 (solid circles)

tion, and not the $(V - I)_0 = f(M_I, [\text{Fe}/\text{H}])$ function, since the latter one would be double-valued for the brightest part of the metal rich clusters' RGBs. This choice implies that our fits are not well-constrained for the vertical part of the giant branch, i.e. for magnitudes fainter than $M_I \sim -1$. However, we show in the next section that our analytic function is good enough for the intended purpose, i.e. to obtain the $[\text{Fe}/\text{H}]$ of the RGB stars in far Local Group populations, and thus to analyze how they are distributed in metallicity.

Our synthetic RGB families are plotted in Figs. 6 and 7, for the LDZ distance scale. In the former figure, the ZW metallicity scale is used, while the CG scale is used in the latter one. The figures show that the chosen functional form represents a very good approximation to the true metallicity "distribution" of the RG branches. The *rms* values are smaller than the typical un-

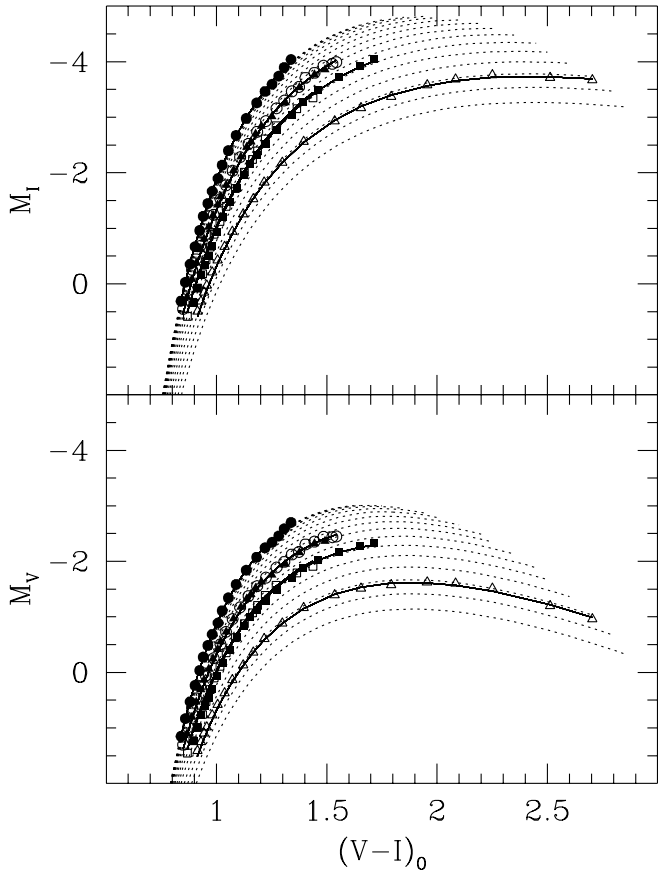


Fig. 7. Same as Fig. 6, for the CG metallicity scale. The metallicity step between the analytic RGBs (dashed lines) is again 0.2 dex. If compared to the previous figure, the non-linear trend of the RGB color with $[\text{Fe}/\text{H}]$ can be clearly seen

certainties in the distance moduli within the Local Group. We further stress the excellent consistency of the empirical fiducial branches for clusters of similar metallicity. We have two pairs of clusters whose metallicities differ by at most 0.03 dex (depending on the scale): NGC 288 and NGC 5904 on the one side, and NGC 5272 and NGC 6205 on the other side. The figures show that the fiducial line of NGC 288 is similar to that of NGC 5904, and the NGC 5272 fiducial resembles that of NGC 6205, further demonstrating both the homogeneity of our photometry and the reliability of the procedure that is used in defining the cluster ridge lines.

If the coefficients of the hyperbolae are taken as third order polynomials, the resulting fits are apparently better (the *rms* is ~ 0.05 mag); however, the trends of the metallicity indices show an unphysical behavior, which is a sign that further clusters, having metallicities not covered by the present set, would be needed in order to robustly constrain the analytic function.

In the following section, the indices are calibrated in terms of metallicity, so that in Sect. 7 they will be used to check the reliability of our generalized fits.

Table 5. The coefficients that define the functions used to interpolate our RGBs (see text); the top header line identifies the two distance scales used, while the two metallicities are identified in the second line of the header

	LDZ		C99	
	CG	ZW	CG	ZW
d	0.212	0.182	0.212	0.182
k1	-0.231	-1.338	-0.227	-1.336
k2	3.290	-0.069	3.314	-0.055
k3	-7.229	-9.547	-7.140	-9.465
k4	0.611	0.710	0.612	0.709
k5	0.551	0.883	0.556	0.881
k6	1.398	1.651	1.401	1.650
k7	0.380	0.525	0.381	0.524
k8	-0.135	0.206	-0.133	0.204
k9	6.194	6.806	6.195	6.805
rms	0.07	0.08	0.07	0.08

Table 6. Coefficients of the calibrating relations for the indices (see text for the definition of the equations). NGC 6656 was excluded from the fits

index	d.sc.	metallicity	α	β	γ	rms	fit
S		CG	-0.03	0.23	-1.19	0.13	2
		ZW	-0.004	-0.18	0.08	0.12	2
		ZW	-0.24	0.28		0.12	1
$(V - I)_{-3.5}$	LDZ	CG	0.00487	-0.0057		0.13	z
		ZW	-2.12	8.81	-9.75	0.13	2
	C99	CG	0.0045	-0.0053		0.15	z
		ZW	-2.05	8.57	-9.61	0.12	2
$(V - I)_{-3.0}$	LDZ	CG	0.0068	-0.0076		0.15	z
		ZW	-3.34	12.37	-11.91	0.14	2
	C99	CG	0.0065	-0.0073		0.15	z
		ZW	-3.233	12.23	-11.96	0.14	2
$\Delta V_{1.4}$		CG	-0.34	0.93	-1.37	0.16	2
		ZW	-0.063	-0.56	0.41	0.16	2
		ZW	-0.87	0.77		0.16	1
$\Delta V_{1.2}$		CG	-0.36	0.55	-0.97	0.19	2
		CG	-0.69	0.0007		0.22	1
		ZW	-0.13	-0.38	-0.28	0.20	2
		ZW	-0.82	0.06		0.20	1
$\Delta V_{1.1}$		CG	-0.30	0.09	-0.81	0.23	2
		CG	-0.59	-0.52		0.25	1
		ZW	-0.13	-0.42	-0.68	0.25	2
		ZW	-0.70	-0.56		0.25	1
$(V - I)_{0,g}$		CG	4.25	-5.37		0.32	1
		ZW	5.25	-6.52		0.33	1

5. Calibration of the indices. Introduction

In order to obtain analytic relations between the indices and the actual metallicity, our photometric parameters were compared both with the ZW and the CG values. A summary of the resulting equations is given in Table 6. For each index (first column) both linear and quadratic fits were tried, of the form: $[Fe/H] = \alpha \cdot \text{index} + \beta$ and $[Fe/H] = \alpha \cdot \text{index}^2 + \beta \cdot \text{index} + \gamma$.

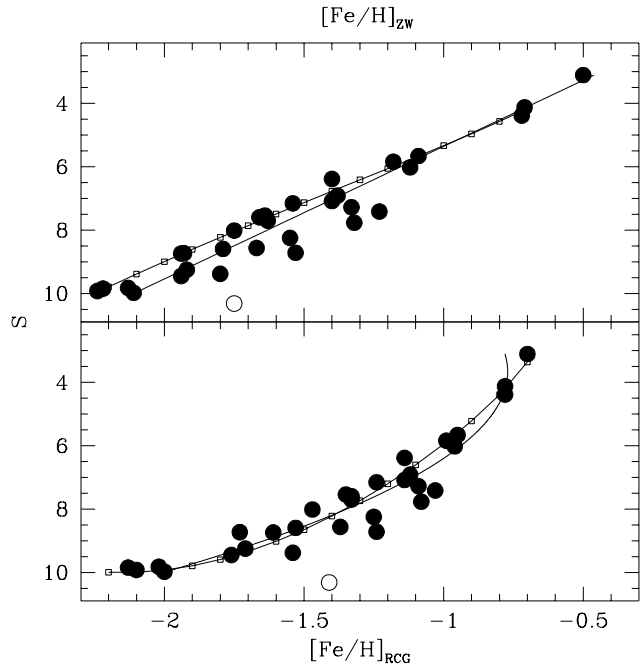


Fig. 8. Calibration of the index S (cf. Fig. 1, left panel) as a function of $[Fe/H]$ on the Zinn & West (1984) scale (top panel) and on the Carretta & Gratton (1997) scale (bottom panel). Linear (top panel) and parabolic (bottom panel) fits of the data are also represented. The cluster marked with open circle was excluded from the fit (see text for details). Starting from this figure (to Fig. 11), the open squares connected by a solid line represent the mono-parametric approximation (see Sect. 4)

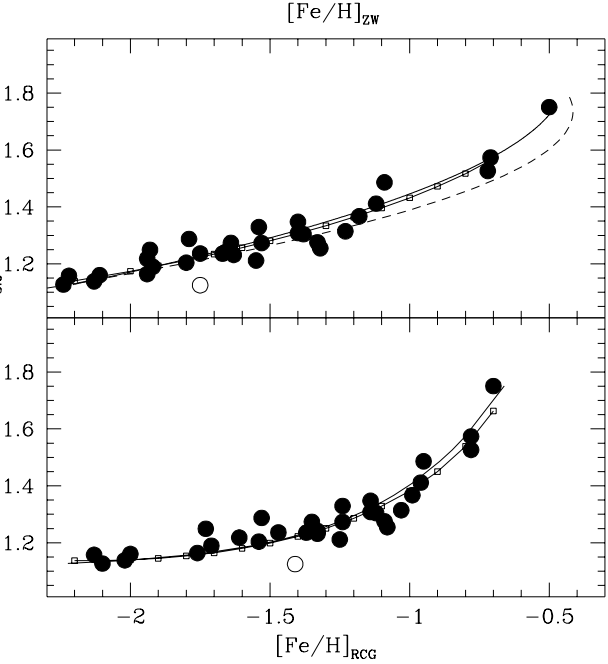


Fig. 9. Calibration of the index $(V - I)_{-3.0}$. The solid lines represent the equations described in the text, while the dashed curve represents the DA90 calibration.

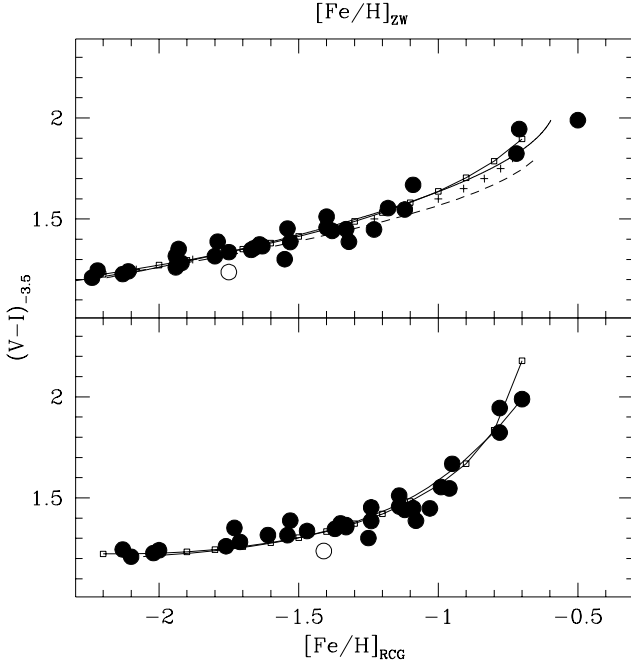


Fig. 10. Calibration of the index $(V - I)_{-3.5}$. The solid lines represent the equations described in the text, while the dashed curve represents the the Lee et al. (1993) calibration. The Caldwell et al. 1998 relation is also shown with plus symbols

The coefficients of the calibrating relation are given in the columns labelled α , β , and γ ; in column 7, the *rms* of the residuals is also given. In the case of the $(V - I)_{-3.0}$ and $(V - I)_{-3.5}$ indices, neither the linear nor the quadratic fits give satisfactory results, when the CG scale is considered. Instead, a good fit is obtained if a change of variables is performed, setting $z = 0.02 \times 10^{[\text{Fe}/\text{H}]}$, and linearly interpolating in the index (i.e. setting $z = \alpha \cdot \text{index} + \beta$). The column 8 of Table 6 identifies the kind of fitting function that is used for each parameter/metallicity combination: the symbols “1”, “2” and “z” refer to the linear, quadratic, and linear in z fits, respectively. Relations on both the CG and ZW metallicity scales are given, and column 3 flags the $[\text{Fe}/\text{H}]$ scale that is used.

In order to measure the $(V - I)_{-3}$ and $(V - I)_{-3.5}$ indices (cf. Sect. 3) a distance scale must be adopted. The most straightforward way is to use the observed V_{HB} (cf. Table 1) coupled with a suitable law for the HB absolute magnitude.

It has become customary to parameterize this magnitude as $M_V(\text{HB}) = a \cdot [\text{Fe}/\text{H}] + b$, although there is no consensus on the value of the two parameters a and b . The current calibrations of these two metallicity indices were obtained by Da Costa & Armandroff (1990) and Lee et al. (1993), and they are based on the Lee et al. (1990; LDZ) theoretical luminosities of the HB. LDZ gave a relation $M_V(\text{HB}) = 0.17 \cdot [\text{Fe}/\text{H}] + 0.82$ valid for $Y = 0.23$.

As discussed in Sect 4, since many current determinations of Population II distances within the Local Group are based on the Lee et al. (1990) distance scale, and for the purpose of comparison with previous studies, we provide a calibration us-

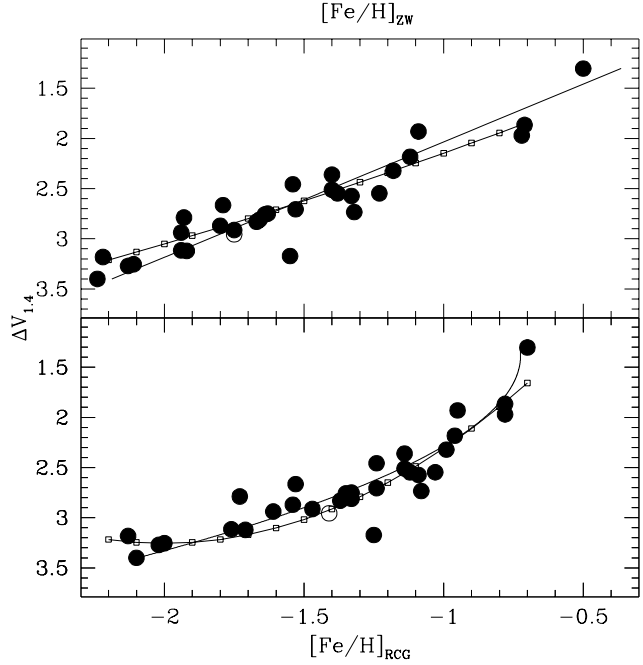


Fig. 11. Calibration of the index $\Delta V_{1.4}$. The solid lines represent linear (top panel) and quadratic (bottom panel) fits to the data

ing the latter HB luminosity-metallicity relation. However, in the last ten years revisions of this relation have been discussed by many authors, so we also calibrated the two indices using $M_V(\text{HB}) = 0.18 \cdot [\text{Fe}/\text{H}] + 0.90$ (Carretta et al. 1999), which is one of the most recent HB-based distance scales.

We must stress that *metallicities on the ZW scale must be used in the M_V vs. $[\text{Fe}/\text{H}]$ relation*. Indeed, CG showed that their scale is not linearly correlated to that of ZW, so not even the M_V vs. $[\text{Fe}/\text{H}]$ relation will be linear: if one wishes to use the new scale, then *the absolute magnitude of the HB must be re-calibrated* in a more complicated way.

The best calibrating relations are shown in Figs. 8 to 11. In the following sections, for each index a few remarks on the accuracy of the calibrations and comparisons with past studies are given.

6. Calibration of the indices. Discussion

6.1. S

On the CG scale, the second-order fit has a residual *rms* of 0.12 dex in $[\text{Fe}/\text{H}]$. On the ZW scale, the linear fit is obtained with a *rms* of 0.12 dex. This index can therefore be calibrated on both scales, with a comparable level of accuracy. A parabolic fit does not improve the relation on the ZW scale, since the coefficient of the quadratic term is very small (-0.004) and the *rms* is the same. These relations are shown in Fig. 8 as solid lines, where the upper panel is for the ZW scale, and the lower panel for the CG scale (this layout is reproduced in all the following figures).

The cluster NGC 6656 (M22) was excluded from the fits, and is plotted as an open circle in Fig. 8. It is well-known that M22 is a cluster that shows a metallicity spread, and indeed it falls outside the general trend in most of the present calibrations.

6.2. $(V - I)_{-3.0}$

The first definition of the $(V - I)_{-3.0}$ index was given in Da Costa & Armandroff (1990), where a calibration in terms of the ZW scale was also given: $[\text{Fe}/\text{H}] = -15.16 + 17.0 (V - I)_{-3} - 4.9 (V - I)_{-3}^2$. The same index (measured on the *absolute* RGBs corrected with the LDZ HB luminosity-metallicity relation) is plotted, in Fig. 9, as a function of the metallicity on both scales, and the solid lines represent our calibrations. The top panel shows the quadratic relation on the ZW scale, whose *rms* is 0.14 dex. The bottom panel of Fig. 9 shows the relation on the CG scale. In this case, a quadratic fit is not able to reproduce the trend of the observational data. A better result can be obtained by making a variable change, i.e. using the variable $z = 0.02 \cdot 10^{[\text{Fe}/\text{H}]}$; in this case, a linear relation is found, and its *rms* is 0.15 dex. This measure of the residual scatter has been computed after transforming back to metallicity, so the reliability of the index can be compared to that of the other ones. Again, the index can be calibrated on both scales with a comparable accuracy. The dashed curve in the upper panel of Fig. 9 shows the original relation obtained by DA90: there is a small discrepancy at the high-metallicity end, which can be explained by the different 47 Tuc fiducial line that was adopted by DA90 (cf. below the discussion on $(V - I)_{-3.5}$).

As already recalled, we checked the effect of adopting another distance scale, by repeating our measurements and fits, and adopting the C99 distance scale. For the ZW metallicity scale, we obtain the quadratic relation whose coefficients are listed in Table 6, and whose *rms* is 0.15 dex. The bottom panel of Fig. 9 shows the relation on the CG scale. Again, a quadratic fit is not able to reproduce the trend of the observational data. Making the already discussed variable substitution, the linear relation in z has an *rms* of 0.16 dex, so the two metallicity scales yield almost comparable results.

6.3. $(V - I)_{-3.5}$

Using the same “standard” GC branches of DA90, Lee et al. (1993) defined a new index, $(V - I)_{-3.5}$, to be used for the farthest population II objects. It was also calibrated in terms of the ZW scale: $[\text{Fe}/\text{H}] = -12.64 + 12.6 (V - I)_{-3.5} - 3.3 (V - I)_{-3.5}^2$. A new calibration was also given recently in Caldwell et al. (1998): $[\text{Fe}/\text{H}] = -1.00 + 1.97 q - 3.20 q^2$, where $q = [(V - I)_{-3.5} - 1.6]$. The index and our calibrations (solid lines) are plotted, in Fig. 10, on both metallicity scales. Again, the measurements were made in the absolute CMD, assuming the LDZ distance scale. Our quadratic calibration vs. the ZW scale has a residual *rms* scatter of 0.13 dex, which is the same of the linear relation on the CG metallicity vs. z .

The Lee et al. relation (dashed line) predicts slightly too larger metallicities on the ZW scale, for $[\text{Fe}/\text{H}] > -1$. This can also be interpreted as if the DA90 47 Tuc branch were < 0.1 mag bluer than ours. Indeed, if one looks at Fig. 5 of DA90, one can easily see that some weight is given to the brightest RGB star, which is brighter than the trend defined by the previous ones. The result is a steeper branch, which also justifies the DA90 slightly bluer RGB fiducial. Since our metal richest point is defined by two clusters, and since the two measured parameters agree very well, we are confident that our calibration is reliable. In any case, the discrepancy between the two scales is no larger than ~ 0.1 dex. It is also reassuring that the Caldwell et al. (1998) relation (pluses) is closer to the present calibration, since the former is based on a larger set of clusters. This might be an indication that the Lee et al. relation is actually inaccurate at the metal rich end, due to the small set of calibrating clusters.

As before, we obtained a further calibration also using the C99 M_V vs. $[\text{Fe}/\text{H}]$ relation; the quadratic fit on the ZW scale has a residual *rms* scatter of 0.13 dex, while the z variable can be fitted with a straight line, with an *rms* of 0.14 dex.

6.4. The ΔV family and $(V - I)_{0,g}$

For any ΔV index, the quadratic relations vs. the ZW metallicity do not improve the *rms* and they are not plotted in the figures. The coefficients are listed in Table 6.

The best metallicity estimates of the “ ΔV family” are obtained with the $\Delta V_{1.4}$ index. The errors on $[\text{Fe}/\text{H}]$ are just slightly larger than the standard uncertainties of the spectroscopic determinations. The solid lines of Fig. 11 show the calibrations that we obtain. The quadratic equation on the CG scale, and the linear one on the ZW scale, are obtained with residual scatters of 0.16 dex.

The rest of the indices in this family, and $(V - I)_{0,g}$, lack the precision of the other abundance indicators. This is due to the fact that the error on any ΔV index is proportional to the uncertainty on the color of the RGB (which depends on the reddening), times its local slope where the reference point is measured. Since the RGB slope increases going away from the tip (i.e. towards bluer colors), we expect that the scatter on the ΔV indices will also increase as the color of the reference point gets bluer. Indeed, Table 6 shows that in most cases the *rms* uncertainties are > 0.2 dex for these indices. The residual scatter is largest for the $(V - I)_{0,g}$ index, which is the most affected by the uncertainties on the reddening.

The $\Delta V_{1.2}$ and $(V - I)_{0,g}$ parameters have been earlier calibrated, on the CG scale, by Carretta & Bragaglia (1998). Using their quadratic relation for $\Delta V_{1.2}$, and both their linear and quadratic relations for $(V - I)_{0,g}$, the corresponding *rms* of the residuals in metallicity are 0.21 dex and ~ 0.41 dex, respectively. Our new and the old calibrations are therefore compatible, within the (albeit large) uncertainties.

7. A test of the “model” RGBs; comparison with the observed [Fe/H] indices

A straightforward test of our new analytic RGBs can be made by generating the same metallicity indices that have been measured on the observed RGBs, and then checking the consistency of the predicted vs. measured quantities. To this aim, for a set of discrete [Fe/H] values a $(V - I)_0$ vector was generated, and the combination of the two was used to compute the M_I vector of the giant branch, using Eqs. (2-6). Then for each branch the metallicity indices were measured as it was done for the clusters’ fiducials.

In Figs. 8 to 11, the predicted indices are identified by the small open squares (spaced by 0.1 dex) connected by a solid line. The best predictions are for those indices that rely on the brightest part of the RGB (i.e. $(V - I)_{-3.0}$, $(V - I)_{-3.5}$ and $\Delta V_{1.4}$), while the computations are partially discrepant for those indices that rely on a point that is measured on the faint RGB. This is easily explained by the nature of our fit: since the best match is searched for along the ordinates (for the reasons discussed in Sect. 4), then it is better constrained in the upper part of the RGB, where its curvature becomes more sensitive to metallicity. We must also stress that the metal richest cluster in the reference grid is 47 Tuc ([Fe/H] = -0.70 on the ZW scale), whereas NGC 6352 ([Fe/H] = -0.50 on the same scale) is the metal richest cluster for which metallicity indices have been measured. Some of the discrepancies that are seen at the highest metallicities are therefore due to the lack of low-reddening clusters that can be used to extend the reference grid to the larger [Fe/H] values.

The mean differences between the predicted and fitted indices are, on the ZW scale, around 0.03 dex for the $(V - I)_{-3.0}$ and $(V - I)_{-3.5}$ indices. They are around 0.08 dex for the $\Delta V_{1.2}$, $\Delta V_{1.4}$, and S indices. They rise to ~ 0.1 and ~ 0.3 dex for the $\Delta V_{1.1}$ and $(V - I)_{0,g}$ indices. A similar trend is seen for the comparison on the CG scale. In this case, the mean differences are ~ 0.05 dex for $(V - I)_{-3.0}$, $(V - I)_{-3.5}$, and S ; they are ~ 0.1 dex for $\Delta V_{1.2}$ and $\Delta V_{1.4}$; and they are 0.12 and 0.27 for the $\Delta V_{1.1}$ and $(V - I)_{0,g}$ indices.

We can therefore conclude that, apart from the $\Delta V_{1.1}$ and $(V - I)_{0,g}$ indices, our mono-parametric RGB family gives a satisfactory reproduction of the actual changes of the RGB morphology and location, as a function of metallicity. It is then expected that, using this approach, one can exploit the brightest ~ 3 mags of the RGB to determine the mean metallicity, and even more important, the metallicity *distribution* of the old stellar population of any Local Group galaxy. In a forthcoming paper, we will demonstrate such possibility by re-analyzing our old photometric studies of the dwarf spheroidal galaxies Tucana (Saviane et al. 1996), Phoenix (Held et al. 1999a; Martínez-Delgado et al. 1999b), Fornax (Saviane et al. 1999a), LGS 3 (Aparicio et al. 1997), Leo I (Gallart et al. 1999; Held et al. 1999b) and NGC 185 (Martínez-Delgado et al. 1999a).

8. Conclusions

In this work, we have provided the first calibration of a few metallicity indices in the $(V - I), V$ plane, namely the indices S , $\Delta V_{1.1}$ and $\Delta V_{1.4}$. Calibrations on both the Zinn & West (1984) and Carretta & Gratton (1997) scales have been obtained. The metallicity indices $(V - I)_{0,g}$, $\Delta V_{1.2}$, $(V - I)_{-3.0}$ and $(V - I)_{-3.5}$ have been also calibrated on both scales, and we have shown that our new relations are consistent with existing ones. In the case of the latter two indices, we have obtained the first calibration on the CG scale; for both scales, we have also obtained the first calibration that takes into account new results on the RR Lyr distances. The accuracy of the calibrations is generally better than 0.2 dex, regardless of the metallicity scale that is used.

Our results are an improvement over previous calibrations, since a new approach in the definition of the RGB is used, and since our formulae are based on the largest homogeneous photometric database of Galactic globular clusters.

The availability of such database also allowed us a progress towards the definition of a standard description of the RGB morphology and location. We were able to obtain a function in the $(V - I)_0, M_I, [\text{Fe}/\text{H}]$ space which is able to reproduce the whole set of GGC giant branches in terms of a single parameter (the metallicity). We suggest that the usage of this function will improve the current determinations of metallicity and distances within the Local Group, extending the methods of Lee et al. (1993).

Acknowledgements. We thank the referee, Gary Da Costa, for helpful suggestions that improved the final presentation of the manuscript. I.S. acknowledges the financial support of Italian and Spanish Foreign Ministries, through an ‘Azioni Integrate/Acciones Integradas’ grant.

References

- Aparicio A., Gallart C., Bertelli G., 1997, AJ 114, 680
- Armandroff T.E., Da Costa G.S., Caldwell N., Seitzer P., 1993, AJ 106, 986
- Bertelli G., Bressan A., Chiosi C., Fagotto F., Nasi E., 1994, A&AS 106, 275
- Buonanno R., Corsi C.E., Pulone L., Fusi Pecci F., Bellazzini M., 1998, A&A 333, 505 (B98)
- Caldwell N., Armandroff T.E., Da Costa G.S., Seitzer P., 1998, AJ 115, 535
- Carretta E., Bragaglia A., 1998, A&A 329, 937
- Carretta E., Gratton R., 1997, A&AS 121, 95 (CG)
- Carretta E., Gratton R.G., Clementini G., Fusi Pecci F., 1999, ApJ, in press (C99)
- Da Costa G.S., Armandroff T.E., 1990, AJ 100, 162 (DA90)
- Dean J.F., Warren P.R., Cousins A.W.J., 1978, MNRAS 183, 569
- Gallart C., Freedman W., Aparicio A., Bertelli G., Chiosi C., 1999, AJ, 118, 2245
- Harris G.L.H., Harris W.E., Poole G.B., 1999, AJ 117, 855
- Harris W.E., 1996, AJ 112, 1487
- Hartwick F.D.A., 1968, ApJ 154, 475
- Held E.V., Saviane I., Momany Y., 1999a, A&A 345, 747
- Held E.V., Saviane I., Momany Y., Carraro G., 1999b, ApJ, in press
- Lee M.G., Freedman W.L., Madore B.F., 1993, ApJ 417, 553

Lee Y.W., Demarque P., Zinn R., 1990, *ApJ* 350, 155 (LDZ)

Lloyd Evans T., 1983, *S. Afr. Astron. Obs. Circ.* 7, 86

Martínez-Delgado D., Aparicio A., Gallart C., 1999a, *AJ*, 118, 2229

Martínez-Delgado D., Gallart C., Aparicio A., 1999b, *AJ*, 118, 862

Rosenberg A., Saviane I., Piotto G., Aparicio A., 1999a, *AJ*, 118, 2306
(RSPA99)

Rosenberg A., Piotto G., Saviane I., Aparicio A., 1999b, *A&AS*, in press

Rosenberg A., Aparicio A., Saviane I., Piotto G., 1999c, *A&AS*, submitted

Rutledge A.G., Hesser J.E., Stetson P.B., 1997, *PASP* 109, 907
(RHS97)

Sandage A., Smith L.L., 1966, *ApJ* 144, 886

Sandage A., Wallerstein G., 1960, *ApJ* 131, 598

Saviane I., Held E.V., Bertelli G., 1999a, *A&A*, in press

Saviane I., Held E.V., Piotto G., 1996, *A&A* 315, 40

Saviane I., Rosenberg A., Piotto G., 1997. In: R.T. Rood, A.Renzini (eds.) *Advances in Stellar Evolution*, Cambridge University Press, Cambridge, p. 65 (SRP97)

Saviane I., Piotto G., Fagotto F., et al., 1998, *A&A* 333, 479

Saviane I., Rosenberg A., Piotto G., 1999b. In: B. K. Gibson, T. S. Axelrod, M. E. Putman (eds.), "The Third Stromlo Symposium: The Galactic Halo" (SRP99)

Walker A., 1992, *PASP* 104, 1063

Zinn R., West M., 1984, *ApJS* 55, 45 (ZW)